Article

JOURNAL OF COMPOSITE MATERIALS

Journal of Composite Materials
2022, Vol. 56(17) 2765–2778

Article reuse guidelines:
sagepub.com/journals-permissions
DOI: 10.1177/00219983221095901
journals.sagepub.com/home/jcm
SAGE

Finite element modelling of the single fibre composite fragmentation test with comparison to experiments

Yanmei Cao[1], Yang Xu[2], Philip Harrison[1], Edward D McCarthy[3] and Daniel M Mulvihill[1]

Abstract

This paper develops a finite element (FE) model of the single fibre fragmentation test designed for direct comparison with experimental results on an E-glass/epoxy system by McCarthy et al. (2015). Interface behaviour is modelled via a cohesive surface, and stochastic Weibull fibre strengths (determined by independent experiments) assigned at random to the elements along the fibre. Predictions from the model agree with experiment for a range of outputs: The evolution of the number of fibre breaks with strain is similar and breaks occur at random locations as required. The model also captures a transition to a Uniform (rather than Weibull) statistical distribution of break locations at later stages of the test consistent with recent experiments. The evolution of the cumulative distribution of fragment lengths is also similar to that of the experiment. In addition, fibre axial stress and interfacial shear stress distributions conform with experimental observation. Correct model predictions of break locations confirm the approach taken on assigning stochastic (Weibull) strengths along the fibre. The effectiveness of the FE model in capturing a number of key aspects of the fragmentation phenomenon suggest its usefulness as a tool in analysing and interpreting fibre fragmentation tests, including back-calculation of interfacial shear strength.

Keywords

Fragmentation, fibre/matrix bond, interfacial strength, finite element analysis, single fibre fragmentation test

Introduction

In fibre-based composite materials, excellent specific strength and stiffness properties are achieved because the reinforcing fibres (usually glass or carbon fibres) confer high stiffness and strength while a relatively low density matrix material (often a polymer) holds the material together. The mechanical properties of the composite clearly depend on the mechanical properties of the constituent fibre and matrix materials, but they are also highly dependent on the properties of the fibre-matrix interface. Essentially, when load is applied to the composite matrix, it is transferred to the fibres via shear stress arising from the inherent strength of the fibre-matrix interface.

Fibre and matrix mechanical properties can be easily determined by conventional tensile testing. However, the properties of the interface are more complex and difficult to access. The main parameter characterising the interface is the fibre-matrix interfacial shear strength (IFSSh). This is clearly a critical parameter: for example, a low-strength interface will tend to debond, while a high-strength interface will tend to remain bonded and transfer more load into the fibres. Key practical uses of the IFSSh include its importance as a key input to micromechanical composite strength and damage models[1,2] and its usefulness as a means for assessing the interfacial strength of various fibre sizing (coating) types.[3,4] Several testing approaches have been proposed to measure fibre-matrix interface behaviour: pull-out tests,[5,6] micro-bond tests,[5,7] micro-indentation tests[8,9]

[1]James Watt School of Engineering, University of Glasgow, Glasgow, UK
[2]School of Mechanical Engineering, Hefei University of Technology, Anhui China
[3]School of Engineering, University of Edinburgh, Edinburgh, UK

Corresponding authorss:
Daniel M Mulvihill, James Watt School of Engineering, University of Glasgow, University avenue, Glasgow G12 8QQ, UK.
Email: Daniel.Mulvihill@glasgow.ac.uk

Yang Xu, School of Mechanical Engineering, Hefei University of Technology, Tianjin, China.
Email: Yang.Xu@hfut.edu.cn

Edward D McCarthy, School of Engineering, University of Edinburgh, Sanderson Building, Kings Buildings, Edinburgh EH9 3JL, UK.
Email: ed.mccarthy@ed.ac.uk

and, the subject of the present paper: the single fibre fragmentation test (SFFT).[10–12] Among these approaches, the SFFT (first proposed by Kelly and Tyson[13]) is considered one of the most insightful as it allows for determination of interface properties *in-situ* while the fibre is fully embedded in a matrix as would be the case in the real composite. In general, the SFFT involves tensile testing of a dog-bone specimen with a single full-length axial fibre embedded along the central longitudinal axis. A matrix material with strain-to-failure of three to four times that of the fibre is generally chosen to ensure fibre breaks occur instead of matrix failure. Carbon and glass fibres are brittle materials containing some stochastic distribution of flaws along their length. When the shear stresses exerted on the fibre by the matrix have built up enough axial stress in the fibre, the fibre will fracture at a flaw location where the stress is sufficient to break the fibre. This process then repeats as the applied global load is increased and local axial stresses at other locations become sufficient to cause further breaks, resulting in the fibre breaking into smaller and smaller fragments. The fibre is said to be stress-saturated when the fragments become so short that shear transfer along their lengths becomes insufficient to generate enough axial stress to cause further breaks even with increased load. At saturation, the number of breaks and fragment lengths are recorded at the final applied strain. The longest fragment length which cannot incur further breaks is called the critical fibre fragment length l_c. An important disadvantage of the method is the fact that the IFFSh cannot be measured directly from the SFFT and has to be back-calculated. Usually, this involves using parameters determined from the SFFT in combination with one of the theoretical models describing the fibre-matrix interaction. Generally, the parameters required are an approximation of the critical fibre fragment length l_c and the strength of the fibre $\sigma_f\{l_c\}$ at the critical fibre fragment length (stochastic fibre strength is length dependent) – both can be determined from the SFFT. Typical examples of theoretical models that have been used include the models introduced by Kelly and Tyson,[14] Cox,[15] Nairn,[16] Wu et al.[17–19] and Okabe and Takeda.[20] However, this means that the calculation of the IFFSh is tied to the idealisations and assumptions implicit in the theoretical models. The problem is that any effective model has to capture a wide range of behaviours including correct interface properties, fibre strength distribution, fibre-matrix debonding, matrix plasticity and matrix damage (i.e., matrix cracking). The theoretical models often focus on specific aspects, but a theoretical treatment becomes extremely complex if all these factors are to be included. Advances in computational capability in recent years make the finite element (FE) method ideal for constructing more comprehensive models of the SFFT that could potentially be used to back-calculate IFFSh more accurately from SFFT data.

A number of interesting contributions have been made to the FE modelling of the SFFT. Budiman et al.[21] developed an axisymmetric elastic model using a non-rigid cohesive surface to define the traction-separation behaviour of the fibre-matrix interface. By incorporating a single pre-existing fibre break, they demonstrated how a critical length taken from the contour plot of principal stress difference could be used (via the appropriate formula) to calculate fibre-matrix interface strength from just a single break. However, more work is required to determine the accuracy of this new method in comparison to the conventional SFFT. Wang et al.[22] developed a fully elastic model to handle the repeating fibre break process in ABAQUS using the user subroutine USDFELD. In Wang el al.,[23] the authors added cohesive zone elements to model the traction separation behaviour of the interface and a matrix damage criterion to simulate matrix cracking in an elastic matrix. These contributions, however, did not incorporate the stochastic distribution of fibre strengths along the fibre as is evident from each new break occurring at the centre of fibre fragments (which is contrary to the random break locations that occur experimentally). FE models that have included the key stochastic (Weibull) distribution of fibre strengths along the length of the embedded fibre include van der Meer et al.[24] and Nishikawa et al.[25] and these models also included matrix plasticity. However, the modelling results in[24] and[25] (and those in[22,23]) were not compared to equivalent SFFT experiments to determine how well the models capture certain key behaviour such as evolution of the distribution of fibre break locations and distribution of fragment lengths during the test (Budiman et al.[21] were concerned only with the first break so did not use their model to study break evolution). In fact, there has been some disagreement concerning the fragment length distributions that have been observed at saturation. Drzal et al.[26] studied an epoxy/carbon fibre system and found good agreement with a Weibull distribution; Netravali et al.[27] found good agreement with a lognormal distribution (also epoxy/carbon); and Bascon and Jensen[28] noted correspondence with a Gaussian distribution for their epoxy/carbon system. Recently, Kim et al.[10] and McCarthy et al.[11] reported on a very high level of agreement (Probability plot correlation coefficient (ppcc) ≥ 0.99) of *break location* data with a uniform distribution for their glass fibre/epoxy SFFT system. They noted that a Uniform distribution of break locations leads to an explicit equation for the ordered *fragment length* distribution due to Whitworth.[29] Clearly there is wide variation in the fragment length data observed and this may be due to obvious variation between materials (fibre & matrix), interface properties and test setups. However, it is important, therefore, that an effective FE model be able to predict the evolution of the distribution of break locations and fragment lengths.

In contrast to previous numerical models that are short and focus on microscopic damage with a constant fibre strength, the length of the present model is equivalent to experimental specimen gauge lengths[11] and the variation of the strength along the embedded single fibre is modelled following an appropriate statistical (Weibull) distribution with experimentally determined distribution parameters. This allows us to compare key model predictions to experimental data (such as distribution of break locations and stress distributions). In addition, the model is designed to mimic the experimental SFFT test setup in McCarthy et al.[11] as closely as possible (i.e., identical properties for the E-Glass fibres and epoxy matrix etc.). The comparison can reflect the degree to which FE modelling can capture the underlying physics in these single fibre fragmentation tests. In summary, the key difference between this work and previous FE modelling work is that the present paper compares the FE result directly with experimental data and is also the first FE paper to study the evolution of the distribution of fibre break locations (and fragment lengths) during the test.

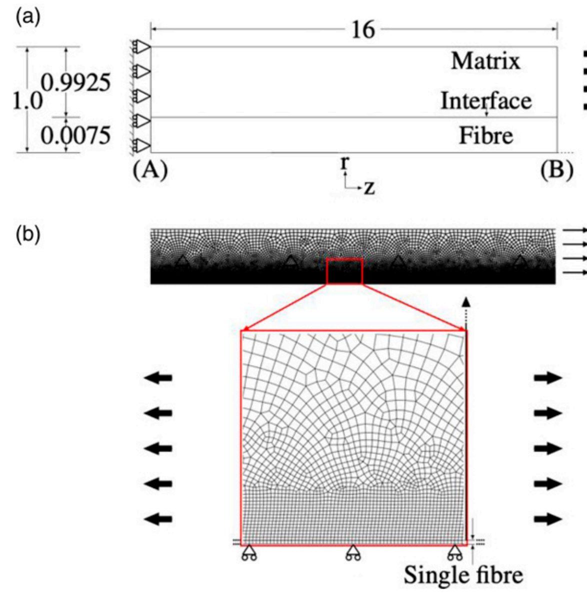

Figure 1. (a) Finite element model schematic and (b) finite element mesh with local inset showing mesh detail.

Numerical simulation

Finite element model

The purpose of the FE model here is to compare FE results with the single fibre fragmentation experiments in McCarthy et al.[11] In McCarthy et al.,[11] the single fibre fragmentation tests were carried out on epoxy dog-bone specimens with E-glass fibres. Fibre break data were recorded optically in the central 16 mm of the gauge length. Here an axisymmetric FE model is used to simulate the 16 mm observation length. The model (developed in ABAQUS Implicit) is illustrated schematically in Figure 1. Boundary conditions (Figure 1(a)) were defined by fixing one end of the model (A) and allowing the fibre axisymmetric boundary to apply along the model length. Tensile elongation is applied to the matrix at the opposite end (B). A mesh dependency analysis was performed to ensure a fine mesh is selected and the mesh details are illustrated in Figure 1(b). The glass fibre mesh is composed of 2133 four-node bilinear 7.5 μm × 7.5 μm elements (CAX4R) – the element size being the same as that of the glass fibre radius (Table 1). Doubling the number of elements in the fibre to 4266 altered the maximum fibre axial stress by only 0.06%. The matrix is meshed with biased and gradually size increased elements and has 844 three-node linear elements (CAX3) in a zone close to the fibre-matrix interface and 59959 four-node bilinear elements (CAX4R) elsewhere.

The fibre was assumed to be mechanically elastic until the onset of damage (see *Fibre damage and stochastic fibre strength*), and the matrix was assumed to be elastic-perfectly plastic. General properties of the fibre and matrix are chosen to be those of McCarthy et al.,[11] and are outlined in Table 1. The properties of the matrix (a DGEBA/m-PDA resin system) are taken directly from,[11] while the general fibre properties are taken from the datasheet for Owens Corning 495 E-glass fibres[30] (as these are the fibres used in McCarthy et al.[11]). For simplicity, viscoelastic effects were not incorporated, and the model was run quasi-statically. Strain was increased by applying 0.75 mm extension increments to the 16 mm gauge length up to 5% strain (which was sufficient to reach saturation of fibre breaks).

Fibre damage and stochastic fibre strength

In the case of the SFFT, the fibre has lower strain-to-failure (than the matrix) and carries most of the applied load, so it is the fibres that begin to fail first. A fibre break happens when the local stress in the fibre exceeds the local strength:

$$\sigma > \sigma_f, \qquad (1)$$

where σ is local fibre axial tensile stress, and σ_f is the local fibre strength. In this paper, according to equation (1), two ABAQUS/Standard user subroutines, USDFLD and GETVRM, are implemented to achieve the fibre breaks. The tensile strength of each fibre element is defined in the USDFLD subroutine, and maximum axial stresses of the fibre elements are recorded in each increment by calling the GETVRM subroutine. When the axial stress in any fibre element exceeds its fibre strength, the fibre element fails and a new fibre break appears. The process is described in the

Table 1. Dimensions and material properties for glass fibre30 and matrix11 as from McCarthy et al.11

Material	Radius (um)	Young's modulus (GPa)	Poisson's ratio	Young's modulus degradation factor (see[22,23])	Yield stress (MPa)
E-glass fibre (Owen corning 495)	7.5	75	0.23	0.0075	See Fibre damage and stochastic fibre strength
Epoxy matrix (DGEBA/m-PDA resin system)	—	3.5	0.3	—	80

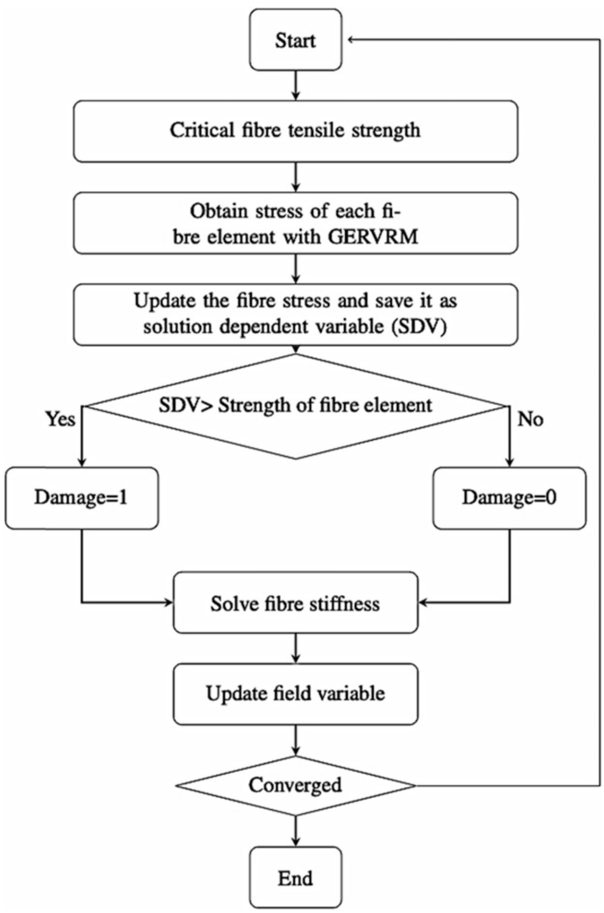

Figure 2. Flowchart for simulating fibre damage process with subroutines USDFLD and GETVRM.

flowchart in Figure 2. In some studies,[22,23] equation (1) has been implemented (with these subroutines) based on a single homogenous strength for the entire fibre, and this results in the somewhat artificial situation where breaks occur at the middle of fragment lengths. Of course, fibres are generally brittle materials having a stochastic distribution of flaws along their length. Fibres will generally fail when the local stress is sufficient to cause a break at a given flaw. Generally, this will be the weakest flaw. Failure then progresses to less weak flaws as the loading is increased. Thus, fibre strength generally follows a stochastic distribution. Generally, it has been found that a two-parameter Weibull strength distribution is effective in describing fibre strength.[31–33]

To implement a Weibull based fibre tensile strength distribution, each fibre element was assigned a tensile strength extrapolated from the Weibull function:

$$P = 1 - exp\left[-\left(\frac{L}{L_0}\right)\left(\frac{\sigma_f}{\sigma_0}\right)^m\right], \tag{2}$$

where P is cumulative probability of failure, σ_f is the fibre tensile strength, L is variable fibre length, L_0 is fibre gauge length, m is the Weibull shape parameter (or modulus) and σ_0 is the Weibull scale parameter. For each element in the fibre, a probability of failure P was randomly (and independently) assigned based on a uniform distribution of probabilities [0, 1]. This reflects the assumption that flaws are equally likely at all locations along the fibre and that the probability of failure is independent at each location.[34] equation (2) was then solved to determine a local fibre strength consistent with the Weibull *strength* distribution and this was assigned to the element. Weibull parameters for the fibres are not reported in McCarthy et al.[11] However, the fibres used in[11] were Owens Corning 495 E-glass fibres.[30] Thus, to obtain usable Weibull parameters, we have tested these fibres in our own laboratory. Single fibre tests (SFT's) were used similar to those in.[35,36] Glass fibres were glued to a paper frame in alignment with the axis of a central diamond shaped gap cut out from the middle (Figure 3(a)). Before applying a tensile load, both sides of the paper frame at mid-gauge were carefully cut so that the load path is entirely through the fibre (Figure 3(b)). The gauge length L_0 was selected at 16 mm - the same as the FE model. Tensile load was then applied until failure. The failure load was divided by the average cross-sectional area (averaged from microscope diameter measurements at 10 locations along the fibre) to give the fibre strength and the test was then repeated to ascertain several fibre strengths.

For a constant gauge length test such as this, equation (2) can be rearranged as:

$$\ln[-\ln(1 - P)] = m\ln(\sigma_f) - m\ln(\sigma_0), \tag{3}$$

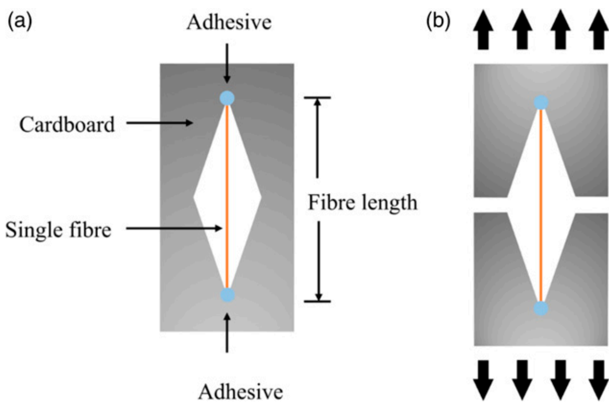

Figure 3. Single fibre test: (a) fibre placement and (b) fibre tensile testing.

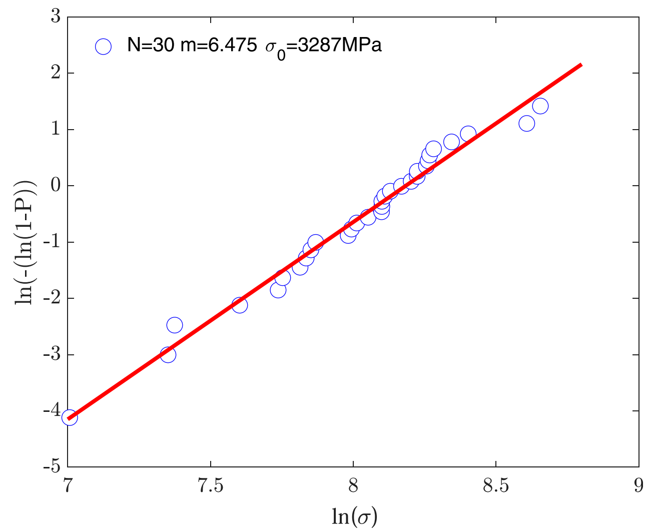

Figure 4. Weibull fitting plot of $\ln[-\ln(1-P)]$ versus $\ln(\sigma)$ for the single fibre E-glass tensile tests. Required Weibull parameters m and σ_0 are determined from the slope and 'y-intercept'.

The test was conducted $N = 30$ times and failure strengths were calculated and sorted in ascending order with a unique rank value j. The cumulative probability is then calculated as[37]:

$$P(j) = \frac{j - 0.5}{N} \tag{4}$$

Fitting a straight line to the plot of $\ln[-\ln(1-P)]$ versus $\ln(\sigma_f)$ (Figure 4) allows determination of the Weibull parameters from the slope and y-intercept. Table 2 shows that the Weibull shape parameter m and scale parameter σ_0 obtained from Figure 4 are reasonable when compared to other results for glass fibres.[31,38–41] The calculated Weibull parameters were then used to generate a list of single fibre tensile strengths for assignment to individual fibre elements in the FE model. Strengths were generated retaining the variable length L as 16 mm in equation (2) as attempting to scale for element size results in drastically unrealistic fibre strengths. In fact, fibre strengths obtained by scaling for element size are so high that they fail to produce any breaks in the SFFT simulation. The scaling overestimation problem is well known – a number of authors have commented on the issue[31,42,43]; however, there remains no straightforward way to reliably scale (or extrapolate) the fibre strengths especially to fibre lengths on the micron scale. The methodology for assigning fibre strengths to fibre elements is illustrated in Figure 5.

Interface behaviour

The interface between a fibre and its surrounding matrix is a flexible (i.e., non-rigid) interface that enables stress transfer from the matrix to the fibre. The interface can transfer increasing amounts of shear stress (as determined by the applied loading) until it reaches a strength limit, which we refer to as the interfacial shear strength (IFSSh).

Table 2. Calculated Weibull parameters (present work) compared to reported values in the literature for single glass fibres.

Shape parameter m	Scale parameter σ_0 (MPa)	Ref.
3.090	1649	38
3.993	2266	39
5.500	3810	31
5.610	2930	40
6.340	1550	41
6.475	3287	Present work

Thus, the interface behaviour can be approximated by a traction-separation law of the type outlined in Camanho et al.[44] Normal and tangential stress at the interface can be defined as being linearly related to interface displacement as:

$$\begin{Bmatrix} t_n \\ t_s \end{Bmatrix} = \begin{Bmatrix} K_{nn} & K_{ns} \\ K_{ns} & K_{ss} \end{Bmatrix} \begin{Bmatrix} \delta_n \\ \delta_s \end{Bmatrix}, \tag{5}$$

where K_{nn}, K_{ss} and K_{ns} are interface stiffnesses (normal, shear and coupled, respectively), δ_n is delamination opening displacement, and δ_s is the relative sliding displacement. To simulate interfacial failure, two damage criteria are introduced: damage initiation and damage evolution. Once the initiation criterion is met, the interface stiffness is degraded with increasing separation until it has fully failed. The full cohesive interface response is shown in Figure 6. A 2D axisymmetric FE analysis is performed in this paper, and hence only normal

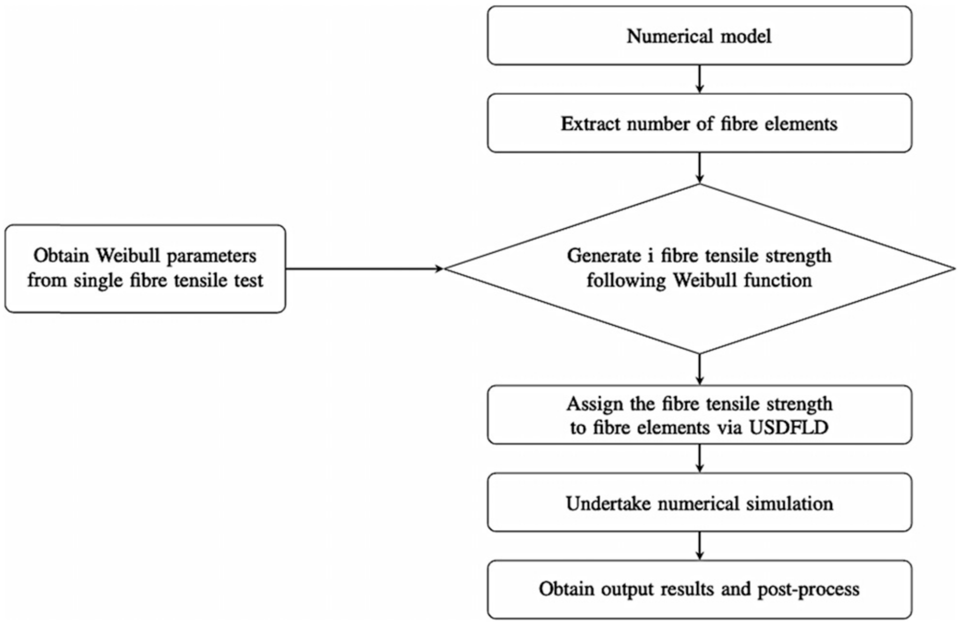

Figure 5. Flowchart for assigning glass fibre strengths to individual fibre elements in the FE model.

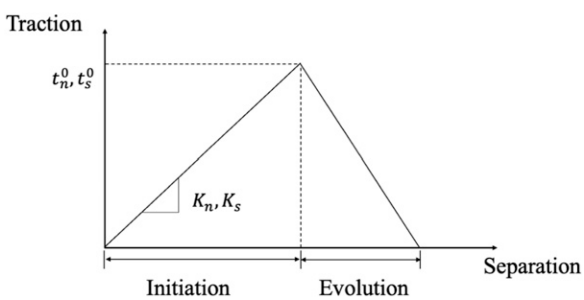

Figure 6. Interfacial traction–separation response for the fibre-matrix interface (t0 is max traction – i.e., strength).

and shear tractions, t_n and t_s, are considered in equation (5).

Damage initiation can be defined based on either interface stresses or displacements. The quadratic stress criterion is employed in this work: that is, the cohesive response begins to degrade once the following relationship between the interface tractions is satisfied:

$$\left\{\frac{<t_n>}{t_n^0}\right\}^2 + \left\{\frac{t_s}{t_s^0}\right\}^2 = 1, \qquad (6)$$

where t_n and t_s are the present normal and shear tractions, and t_n^0 and t_s^0 are the peak values (or strengths) of the interface when only the normal or shear modes are present, respectively. Hence, IFFSh corresponds to t_s^0 in the purely shearing case. The Macaulay brackets $< >$ ensure that the compressive stress state does not initiate damage. Thus, damage initiation involves a coupling between tensile and shear stresses. To define the interface stiffness degradation progress, a scalar parameter D, gradually increasing from 0 to 1, is introduced in the evolution law as:

$$t_n = \begin{cases} (1-D)\bar{t}_n, & \bar{t}_n \geq 0, \\ \bar{t}_n, & \end{cases} \qquad (7)$$

and $\quad t_s = (1-D)\bar{t}_s,$

where $\bar{t}_n$ and $\bar{t}_s$ are the stresses predicted by the elastic traction-separation law for the current strains without damage. Here a fracture energy based linear damage evolution is defined. The critical energy dissipated prior to complete failure G^C is prescribed, thereby defining the area under the curve in Figure 6. When mode mixity is present, the critical energy is defined according to a power law interaction of the energies needed to cause failure in the individual normal and shear directions as:

$$G^C = 1 \Big/ \left(\left\{\frac{G_n}{G_n^C G_T}\right\}^\alpha + \left\{\frac{G_s}{G_S^C G_T}\right\}^\alpha\right)^{1/\alpha}, \qquad (8)$$

where G_n and G_s refer to the present interfacial energy consumed in normal and shear directions, respectively; G_T is the present total energy invested ($G_T = G_n + G_s$) and G_n^C and G_s^C are the critical fracture energies in the normal and shear directions, respectively which require to be prescribed in the model. The cohesive zone is implemented here via a cohesive surface rather than by cohesive elements. The interface properties used in the simulations are given in Table 3. The initial normal and shear interface stiffness

Table 3. Interface properties used in the numerical analysis.

Normal & shear initial stiffness K_n, K_s (N/m^3)	Normal strength t_n^0 (MPa)	Shear strength t_s^0 = IFFSh (MPa)	Shear & normal fracture energy $G_n^C = G_s^C$ (J/m^2)
10^6	3	50	2.9

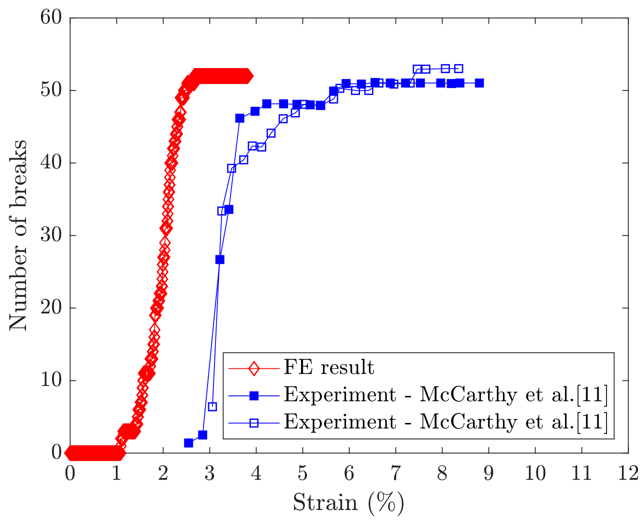

Figure 7. Comparison of number of fibre breaks versus applied strain for the FE model and the experiments of McCarthy et al.[11].

values were set to a sufficiently high value of 10^6 N/m[345] to ensure continuity of the stress and strain fields across fibre and matrix.[46,47] The strength values are taken from experimental work in the literature (normal strength 3 MPa[48] and shear strength 50 MPa[39,49,50]). Reliable data on interfacial fracture energy is more difficult to obtain for the epoxy-glass fibre interface. In this case, the normal and shear fracture energy were adjusted until the number of breaks in the FE model of the SFFT at saturation were comparable with those in the experiments (i.e., McCarthy et al.[11] – see Figure 7). This, of course, implies that the FE model is not yet fully predictive, but the difficulties in obtaining accurate experimental values for some of the input parameters (especially fracture energies) are well known and were also present in previous modelling attempts.[21–24] However, once the model is confirmed to be representative of the experiment (e.g., in terms of number of breaks at saturation), it can be used to study many aspects of the problem (i.e., stress distributions, fibre break statistics etc.). The value (for the critical fracture energy of the interface) arrived at by enforcing agreement of number of breaks at saturation was 2.9 J/m^2

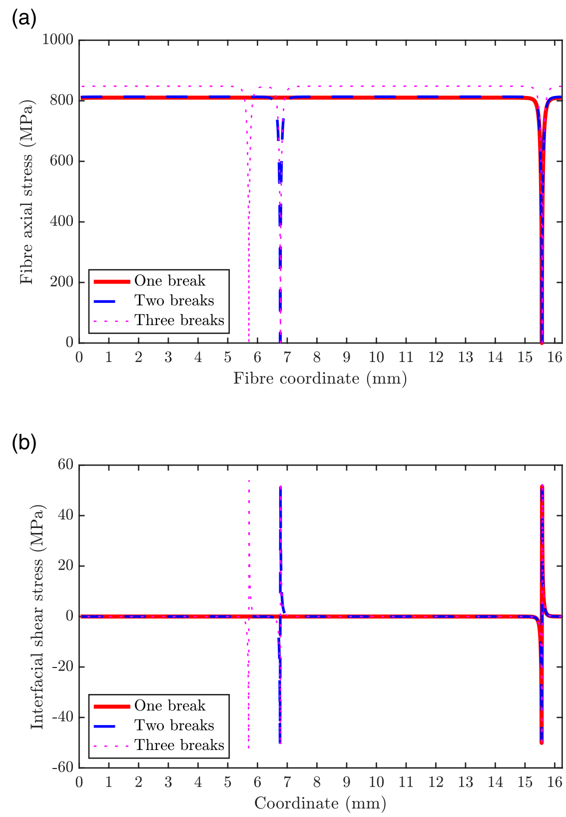

Figure 8. Stress distribution along the fibre gauge length after the first three fibre breaks (a) fibre axial stress (b) interfacial shear stress.

(Table 3) which is within the experimental range of values determined in Varna et al.[51]

Results and discussion

Evolution of fibre breaks and stress distributions

In the FE model, strain was increased incrementally and the fibre break coordinates were recorded. Figure 7 compares the evolution of the number of fibre breaks with applied strain for the FE model devised here with two data sets from the experiments in McCarthy et al.[11] As noted in *Interface behaviour*, the critical fracture energy of the interface in the FE model was tuned until the number of breaks at saturation was nearly equivalent to the experiments (52 breaks in the FE

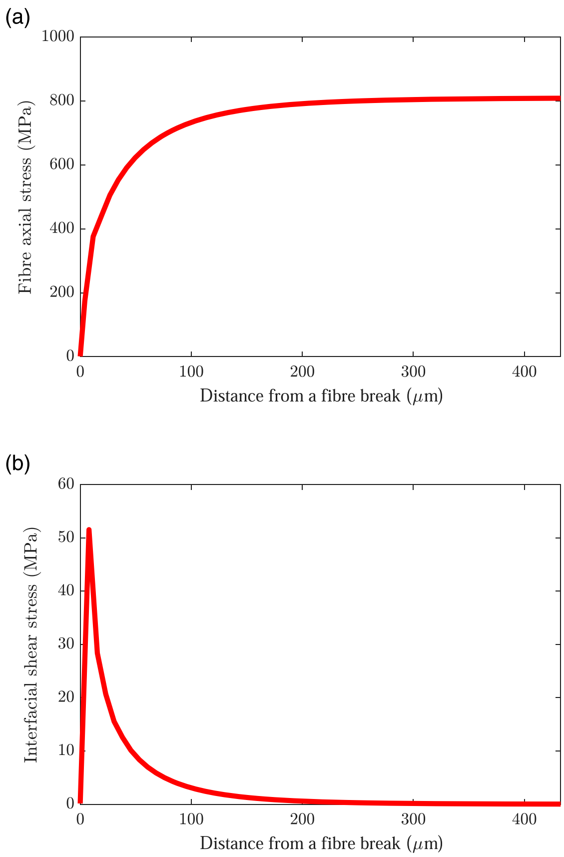

Figure 9. Local FE stress distribtions near a fibre break: (a) fibre axial stress and (b) interficial shear stress.

model and 51 and 53 breaks for the two experimental results). With this equivalence established, we are now able to use the FE model to study a number of aspects of the problem. We note from Figure 7 that the FE break distribution has a similar profile to the experimental profiles, although the strains at which breaks occur are somewhat lower in the FE model. This may be due to the assignment of some weaker fibre strengths in the model (Weibull strength data for the model is derived from several repeat single fibre tests, but the two experimental SFFT results in Figure 7, obviously come from a test on a single embedded fibre). It may also be that the interfacial shear strength in the FE model (50 MPa chosen from glass-fibre/epoxy literature[39,46,47]) was somewhat higher than that in the experiments of McCarthy et al.[11]

To explore the possibility of closing the strain gap between model and experiment further, we carried out a simple parametric study to examine the effect of fibre-matrix interface properties on the resultant fibre break evolution. The influence of interfacial normal strength, interfacial shear strength and critical fracture energy were investigated by varying each one over three alternative values while holding the other two constant (at the default values used in the paper: $t_n^0 = 3$ MPa, IFFSh or $t_s^0 = 50$ MPa and $G_n^C = G_s^C = 2.9$ J/m^2). The result (given as Figure A1 in the Appendix) essentially shows that the interface properties (at least over the ranges investigated) had minimal influence on the evolution of fibre breaks although there were some minor differences between number of breaks at saturation. The important point to note however is that altering the interface properties had little effect on closing the strain gap between model and experiment. As explained above, the gap in Figure 7 is likely due to the fibres in the FE model being somewhat weaker than the (single) fibre used in the McCarthy et al. experiments (due to how the Weibull strength data for the FE model was obtained from multiple single fibre tests; thereby, increasing the possibility of admitting results from weaker fibres).

Figure 8 shows the distribution of both fibre axial stress and interfacial shear stress along the fibre gauge length after each of the first three fibre breaks. Instead of breaking at the geometric centre of fibre fragment lengths (as occurred in Wang et al.,[22,23] where the fibre had a constant strength), breaks appear at "random" locations along the glass fibre – this is a consequence of the assignment of stochastic fibre strengths along the fibre (consistent with the reality of a stochastic distribution of flaws along brittle fibres). In addition, key aspects of the stress distributions are consistent with experimental observation. To aid the discussion, the local stress distributions near a fibre break are magnified in Figure 9. Shear stress is zero at a fragment end, then rises to a peak before assuming a near zero value along most of the fibre length (Figure 8(b) and Figure 9(b)). The non-zero interfacial shear stresses near the fragment ends induce an increase in fibre axial stress from zero at the ends to a near constant value for the rest of the fibre length (Figure 8(a) and Figure 9(a)). The length over which this occurs is often called the stress recovery length. As elongation increases, the fibre stress becomes sufficient to induce new breaks, and the fibre axial stress redistributes along the fibre fragment, taking on an increased maximum axial stress. The break process saturates when the fragments become sufficiently short, such that the stress recovery regions from each end meet and prevent the fibre stress from reaching the breaking stress in the fragment. The profiles in Figures 8 and 9 are consistent with the fibre equilibrium equation[1] $\left(\frac{d\sigma}{dy} = -\frac{2t_s}{r}\right)$ and with the form of the stress profiles measured experimentally using Raman spectroscopy in studies such as Schadler and Galiotis.[52] This is one of the advantages of the FE approach – for example, neither the Cox[15] nor the Kelly-Tyson[14] models correctly capture the experimentally observed shear stress distribution near a

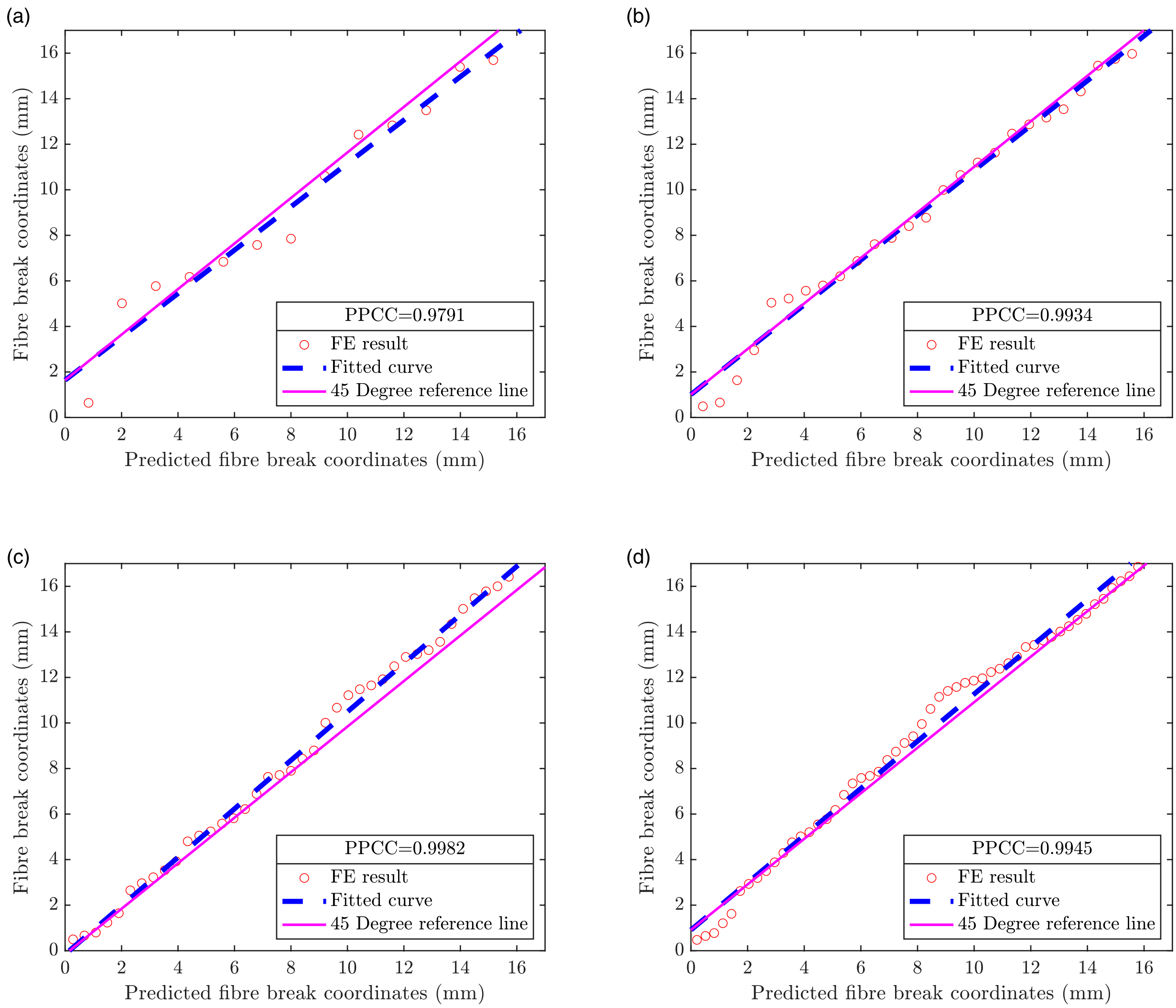

Figure 10. Uniform probability plots of single glass fibre break coordinates from the FE model: (a) 13 fibre breaks at 1.73% strain, (b) 26 fibre breaks at 1.99% strain, (c) 39 fibre breaks at 2.15% strain and, (d) 52 fibre breaks at 2.94% strain. Break coordinates from the FE model (vertical axis) are plotted against predicted break coordinates obtained from uniform median order statistics (horizontal axis).

break in a bonded fibre (i.e., zero at the ends, a peak and a reduction to zero as in Figure 9(b)).

Distribution of fibre break coordinates

The spatial distribution of fibre break coordinates along the single embedded glass fibre is examined next. This is important as it determines the fragment length distribution. Here, there has been recent experimental evidence[10,11] to suggest that the distribution of break locations evolves towards strong correlation with the Uniform distribution after a certain number of breaks (at least for the E-glass/epoxy system in[10,11]). Therefore, we test the goodness-of-fit of the Uniform distribution to the break data from the FE model at various strain levels. The uniform probability plot which graphs percentiles of the data against percentiles of the standard Uniform distribution is adopted. Figure 10 shows the FE break coordinates plotted against predicted fibre break coordinates having a Uniform distribution (and rescaled to the units of the data). The ordered break coordinates are graphed against standard uniform order statistic medians by using Uniform order statistic medians as:

$$m_n = \begin{cases} 1 - m_n & i = 1, \\ \dfrac{i - 0.3175}{n + 0.365} & 2 < i < n - 1, \\ 0.5^{\frac{1}{n}} & i = n, \end{cases} \tag{9}$$

where n refers to the number of fibre breaks, the minimum fibre break coordinate is the first order statistic and the maximum fibre break coordinate is the n$^{\text{th}}$ order statistic. The details of the Uniform order statistic medians are described in Filliben.[53] The quality of the fit is identified by the probability plot correlation coefficient (PPCC).[53] There is assumed to be a high level of agreement of the break coordinates with the uniform distribution when the value of PPCC is greater than 0.99. The uniform probability plots of fibre break coordinates are empirically fitted and the empirical curves are compared with 45° reference lines in Figure 10 (45° indicating perfect agreement with the Uniform distribution). We can see that, beyond about 26 fibre breaks (Figure 10(b)) there is close adherence to the 45° line and the PPCC value is greater than 0.99. This indicates that, beyond a certain stage in the test, the break location data evolves towards the uniform distribution. This is consistent with what both Kim et al.[10] and McCarthy et al.[11] observed experimentally (in McCarthy et al.,[11] the PPCC was in excess of 0.99 from about 31 breaks). The implication of the Uniform distribution of break locations is that break coordinates tend to be spaced equally along the fibre and that breaks are equally likely at all locations -i.e., there is no preferential location for breaks to occur. What is interesting here is that the FE model has produced the same evolution of spatial distribution of breaks as has been observed experimentally. This allows us to make some observations about what leads to this result. The reason for this transition to a Uniform distribution is probably similar in model and experiment. Early in the test, there are just a few breaks and their location will be governed by the Weibull fibre strength distribution (i.e., the weakest flaws fail first). As noted by Kim et al.,[10] the small size of the data set and the existence of weak flaws will lead to variability in the early break statistics. However, noting that flaws are equally likely at each location along a brittle fibre[33] (despite their strength), as the sampling number of breaks increases, we might expect to see a transition to breaks being equiprobable along the fibre – i.e., a Uniform distribution. This is indeed what is observed experimentally. The existence of the same result in the FE model allows us to probe the model inputs that lead to this result. In the model (*Fibre damage and stochastic fibre strength*), each element is first assigned an independent

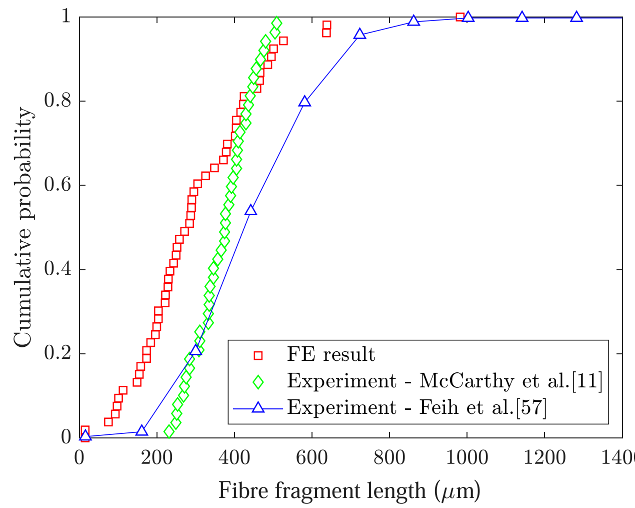

Figure 11. Comparison of cumulative fragment length distributions (at saturation) for the FE model (glass fibre-epoxy, 52 breaks) and experimental results from McCarthy el al.11 (glass fibre-epoxy, 45 breaks) and Feih et al.54 (glass fibre-polyester, 39 breaks). Gauge length was 16 mm in each case.

and random probability of failure P [0, 1] from a Uniform distribution. This reflects the fact that flaws are equally likely at all locations and that failure probability (flaw severity) is independent of location.[33] A fibre strength σ_f determined from the Weibull distribution of fibre strengths is then assigned to the element by solving equation (2) for σ_f. Hence, early in the FE test, break locations are governed by the Weibull strength distribution, but as more breaks occur, the equiprobability of breaks at any location dominates and the data can be expected to evolve to a Uniform distribution. The equivalence of experimental and modelling results with regard to distribution of breaks suggest that the approach taken to assigning local fibre strengths in the FE model is satisfactory – i.e., correctly accounting for the stochastic Weibull distribution of strengths and the equal likelihood of flaws along the fibre.

Distribution of fragment lengths

As has already been noted in McCarthy et al.[11] and Kim et al.,[10] the mathematical consequence of a Uniform distribution of break locations is a fragment length distribution due to Whitworth[29,54–56] (see Appendix in Kim et al.[10] for the distribution equation). What is interesting for us here is to compare the FE distribution of fragment lengths to experiment. Figure 11 compares cumulative fragment length distributions (at saturation) for the FE model with an experimental glass fibre-epoxy result from McCarthy et al.[11]

Although not directly comparable, a glass fibre-polyester result from Feih et al.[57] is also included for comparison. Firstly, the scale of fragment lengths produced by the model (fragments ranging from 15 to 466 μm) is roughly in agreement with the magnitudes in the experiments (see Figure 11). The form of the FE and experimental curves are similar although there is some discrepancy in relation to the position (mean) and spread (variation) of the data. In general, narrow distributions of fragment lengths are thought to be attributable to a narrow underlying fibre strength distribution while lower mean critical fragment length (i.e., a distribution shifted to the left) indicates higher interfacial shear stress transmission.[3,4] Here, the FE glass fibre-epoxy result exhibits a wider spread than the experimental glass fibre-epoxy result (McCarthy et al.[11]). This may be due to a wider spread in the fibre strength distribution because the results in McCarthy et al. come from a fragmentation test on a single embedded fibre sample; whereas, numerous (ex-situ) single fibre tests (SFTs) were performed to determine the Weibull strength statistics for the glass fibre in the FE model. The FE result also yields a somewhat shorter mean critical fragment length of 309.2 μm compared to 370 μm for McCarthy et al.[11] This suggests that the interfacial shear strength in the FE model (50 MPa chosen from glass-fibre/epoxy literature[39,49,50]) may have been somewhat higher than the actual interface strength in McCarthy et al.[11] (which was not reported). The presence of shorter fragment lengths in the FE case also indicates a stronger interface. Turning to the experimental glass fibre-polyester result (Feih et al.[57]), the spread is even larger. Again, this can be attributed to more variation in the fibre strength statistics. In this case, we can assess this directly as the Weibull modulus for the fibres used in the FE model and the fibres in Feih et al.[57,54] are both available. The Weibull modulus was 6.8 (see Table 2) for the fibres modelled in the FE study here, but only 4.4 in Feih et al. – a smaller Weibull modulus indicates a wider spread of the fibre strength data.

Conclusions

The paper develops an FE model of the single fibre fragmentation test (SFFT) for direct comparison with the experimental results in McCarthy et al.[11] (i.e., an E-glass fibre embedded in an epoxy matrix). A cohesive surface is used to model interface behaviour, and a Weibull distribution of fibre strengths (determined by single fibre tests on the E-glass fibres) is implemented in the model by assigning strengths from the distribution to the elements along the fibre. It remains difficult to access accurate experimental data on all input parameters. In this case, the fracture energy of the interface was not accessible, so this was adjusted to provide an equivalent number of fibre breaks (at saturation) as the experiment. With equivalent break numbers at saturation established, the model was then used to successfully study a number of key aspects of the problem. Of particular interest is the fact that the model correctly captures a number of important experimentally observed outcomes. The form of the evolution of fibre break numbers with strain is roughly in agreement with experiment and fibre breaks occur at random locations along the fibre as required. In addition, the distribution of fibre break locations evolves towards good agreement with a Uniform distribution at some point in the test (26 fibre breaks & 2% strain here), but conforms to different distributions earlier in the test. This agrees with recent experimental observations by Kim et al.[10] and McCarthy et al.[11] The form of the cumulative fragment length distribution from the FE model is also roughly in agreement with experiment. The effectiveness of the model in capturing experimentally observed fibre break statistics confirms the usefulness of the approach taken here to assigning stochastic fibre strengths to elements in the FE model (i.e., the probability of failure being independent at each element and local strength being assigned from the appropriate Weibull distribution of strengths). The fibre axial stress and interfacial shear stress distributions are also consistent with experiments both along the fibre and close to breaks.

Theoretical models are often used to back-calculate interfacial shear strength (IFSSh) from SFFTs in the assessment of the fibre-matrix interface; however, such models cannot capture the range of key behaviours which can be included in an FE model. Correct model predictions on each of the aspects studied here (break statistics, stress distributions etc.) suggest FE modelling can play an important role in the analysis of fibre fragmentation tests including replacing theoretical approaches to aid more accurate calculation of IFSSh. However, much more work is required to experimentally determine sufficiently accurate input parameters (such as interfacial fracture energy) to make these models fully predictive.

Acknowledgements

The authors gratefully acknowledge Owens Corning for providing the glass fibres.

Declaration of conflicting interests

The author(s) declared no potential conflicts of interest with respect to the research, authorship, and/or publication of this article.

Funding

The author(s) received no financial support for the research, authorship, and/or publication of this article.

ORCID iD

Daniel M Mulvihill https://orcid.org/0000-0003-1693-0088

Note

1. σ is fibre axial stress, t_s is interfacial shear traction, y is axial length, r is fibre radius.

References

1. Goda K, Miwa Y and Kodama H. Effect of IFSS on tensile strength of unidirectional fiber composites using 3D-FEM simulation. *Adv Compos Mater* 2003; 12(1): 73–89.
2. Vaughan T and McCarthy C. Micromechanical modelling of the transverse damage behaviour in fibre reinforced composites. *Compos Sci Tech* 2011; 71(3): 388–396.
3. Zafeiropoulos NE, Baillie CA and Hodgkinson JM. Engineering and characterisation of the interface in flax fibre/polypropylene composite materials. Part II. The effect of surface treatments on the interface. *Compos Part A: Appl Sci Manuf* 2002; 33(9): 1185–1190.
4. Fraser WA, Ancker FH, Dibenedetto AT, et al. Evaluation of surface treatments for fibers in composite materials. *Polym Compos* 1983; 4: 238–248.
5. Yang L and Thomason JL. Interface strength in glass fibre–polypropylene measured using the fibre pull-out and microbond methods. *Compos Part A: Appl Sci Manuf* 2010; 41(9): 1077–1083.
6. DiFrancia C, Ward TC and Claus RO. The single-fibre pull-out test. 1: review and interpretation. *Compos Part A: Appl Sci Manuf* 1996; 27(8): 597–612.
7. Liu B, Liu Z, Wang X, et al. Interfacial shear strength of carbon fiber reinforced polyphenylene sulfide measured by the microbond test. *Polym Test* 2013; 32(4): 724–730.
8. Desaeger M and Verpoest I. On the use of the micro-indentation test technique to measure the interfacial shear strength of fibre-reinforced polymer composites. *Compos Sci Tech* 1993; 48(1): 215–226.
9. Ho H and Drzal LT. Evaluation of interfacial mechanical properties of fiber reinforced composites using the micro-indentation method. *Compos Part A: Appl Sci Manuf* 1996; 27(10): 961–971.
10. Kim J, Leigh S and Holmes G. E-glass/DGEBA/m-PDA single fiber composites: new insights into the statistics of fiber fragmentation. *J Polym Sci Part B: Polym Phys* 2009; 47(23): 2301–2312.
11. McCarthy ED, Kim JH, Heckert NA, et al. The fiber break evolution process in a 2-D epoxy/glass multi-fiber array. *Compos Sci Tech* 2015; 121: 73–81.
12. Tripathi D and Jones FR. Single fibre fragmentation test for assessing adhesion in fibre reinforced composites. *J Mater Sci* 1998; 33(1): 1–16.
13. Kelley A and Tyson WR. Tensile properties of fiber-reinforced metals. *J Mech Phys Sol* 1965; 13: 329–350.
14. Kelley A and Tyson WR. Fiber-strengthened materials. *J Mech Phys Sol* 1963; 199.
15. Cox HL. The elasticity and strength of paper and other fibrous materials. *Br Journal Applied Physics* 1952; 3(3): 72.
16. Nairn JA. A variational mechanics analysis of the stresses around breaks in embedded fibers. *Mech Mater* 1992; 13(2): 131–154.
17. Wu W, Desaeger M, Verpoest I, et al. An improved analysis of the stresses in a single-fibre fragmentation test: I. Two-phase model. *Compos Sci Tech* 1997; 57(7): 809–819.
18. Wu W, Verpoest I and Varna J. An improved analysis of the stresses in a single-fibre fragmentation test—II. 3-phase model. *Compos Sci Tech* 1998; 58(1): 41–50.
19. Wu W, Verpoest I and Varna J. A novel axisymmetric variational analysis of stress transfer into fibreS through a partially debonded interface. *Compos Sci Tech* 1998; 58(12): 1863–1877.
20. Okabe T and Takeda N. Estimation of strength distribution for a fiber embedded in a single-fiber composite: experiments and statistical simulation based on the elasto-plastic shear-lag approach. *Compos Sci Tech* 2001; 61(12): 1789–1800.
21. Budiman BA, Takahashi K, Inaba K, et al. Evaluation of interfacial strength between fiber and matrix based on cohesive zone modeling. *Compos Part A: Appl Sci Manuf* 2016; 90: 211–217.
22. Wang X, Zhang B, Du S, et al. Numerical simulation of the fiber fragmentation process in single-fiber composites. *Mater & Des* 1980–2015; 31(5): 2464–2470.
23. Wang X, Zhang J, Wang Z, et al. Finite element simulation of the failure process of single fiber composites considering interface properties. *Compos Part B: Eng* 2013; 45(1): 573–580.
24. Van der Meer FP, Raijmaekers S and Rocha IBCM. Interpreting the single fiber fragmentation test with numerical simulations. *Compos Part A: Appl Sci Manuf* 2019; 118: 259–266.
25. Nishikawa M, Okabe T, Takeda N, et al. Micromechanics of the fragmentation process in single-fiber composites. *Model Simulation Mater Sci Eng* 2008; 16(5): 055009.
26. Drzal L, Rich M, Camping J, et al. *Proceedings of the 35th Annual Technical Conference of the Reinforced Plastics/Composites Institue*. Society of Plastics Industry Washington, 1980.
27. Netravali AN, Henstenburg RB, Phoenix SL, et al. Interfacial shear strength studies using the single-filament-composite test. I: experiments on graphite fibers in epoxy. *Polym Compos* 1989; 10(4): 226–241.
28. Bascom WD and Jensen RM. Stress transfer in single fiber/resin tensile tests. *The J Adhes* 1986; 19(3–4): 219–239.
29. Whitworth WA. *Choice and Chance*. D. Bell and Company. 1870
30. Owens Corning E-glass datasheet. *Owens Corning Composite Materials*. Toledo, OH: Owens Corning E-glass datasheet 2020.
31. Keshavan MK, Sargent GA and Conrad H. Statistical analysis of the hertzian fracture of pyrex glass using the

Weibull distribution function. *J Mater Sci* 1980; 15, %6(4): 839–844.
32. Andersons J, Joffe R, Hojo M, et al. Glass fibre strength distribution determined by common experimental methods. *Compos Sci Tech* 2002; 62(1): 131–145.
33. Blassiau S, Thionnet A and Bunsell AR. Micromechanisms of load transfer in a unidirectional carbon fibre–reinforced epoxy composite due to fibre failures. Part 1: micromechanisms and 3D analysis of load transfer: the elastic case. *Compos Structures* 2006; 74(3): 303–318.
34. Shioya M and Takaku A. Estimation of fibre and interfacial shear strength by using a single-fibre composite. *Compos Sci Tech* 1995; 55(1): 33–39.
35. Islam F, Joannès S and Laiarinandrasana L. Evaluation of critical parameters in tensile strength measurement of single fibres. *J Composites Sci* 2019; 3(3): 69.
36. Kim JH, Heckert NA, Mates SP, et al. Effect of fiber gripping method on the single fiber tensile test: II. Comparison of fiber gripping materials and loading rates. *J Mater Sci* 2015; 50(5): 2049–2060.
37. El Asloun M, Donnet JB, Guilpain G, et al. On the estimation of the tensile strength of carbon fibres at short lengths. *J Mater Sci* 1989; 24(10): 3504–3510.
38. Feih S, Thraner A and Lilholt H. Tensile strength and fracture surface characterisation of sized and unsized glass fibers. *J Materials Sci* 2005; 40(7): 1615–1623.
39. Moon CK, Holmes GA and McDonough WG. The effect of inter-fiber distance on the interfacial properties in E-glass fiber/epoxy model composites. *J Appl Polym Sci* 2007; 105(6): 3483–3491.
40. Mesquita F, Bucknell S, Leray Y, et al. Single carbon and glass fibre properties characterised using large data sets obtained through automated single fibre tensile testing. *Compos Part A: Appl Sci Manuf* 2021; 145(1359–835X): 106389.
41. Okabe T and Takeda N. Elastoplastic shear-lag analysis of single-fiber composites and strength prediction of unidirectional multi-fiber composites. *Compos Part A: Appl Sci Manuf* 2002; 33(10): 1327–1335.
42. Zhao FM, Okabe T and Takeda N. The estimation of statistical fiber strength by fragmentation tests of single-fiber composites. *Compos Sci Tech* 2000; 60(10): 1965–1974.
43. Gulino R and Phoenix SL. Weibull strength statistics for graphite fibres measured from the break progression in a model graphite/glass/epoxy microcomposite. *J Mater Sci* 1991; 26(11): 3107–3118.
44. Camanho PP, Davila CG and De Moura MF. Numerical simulation of mixed-mode progressive delamination in composite materials. *J Compos Mater* 2003; 37(16): 1415–1438.
45. Sharma AP, Khan SH and Parameswaran V. Experimental and numerical investigation on the uni-axial tensile response and failure of fiber metal laminates. *Compos Part B: Eng* 2017; 125: 259–274.
46. Canal LP, González C, Segurado J, et al. Intraply fracture of fiber-reinforced composites: microscopic mechanisms and modeling. *Compos Sci Tech* 2012; 72(11): 1223–1232.
47. Melro AR, Camanho PP, Andrade Pires FM, et al. Micromechanical analysis of polymer composites reinforced by unidirectional fibres: part II – Micromechanical analyses. *Int J Sol Struct* 2013; 50(11): 1906–1915.
48. Li D, Yang Q-S, Liu X, et al. Experimental and cohesive finite element investigation of interfacial behavior of CNT fiber-reinforced composites. *Compos Part A: Appl Sci Manuf* 2017; 101: 318–325.
49. Tripathi D, Chen F and Jones FR. The effect of matrix plasticity on the stress fields in a single filament composite and the value of interfacial shear strength obtained from the fragmentation test. *Proc R Soc Lond Ser A: Math Phys Eng Sci* 1996; 452(1946): 621–653.
50. Keusch S and Haessler R. Influence of surface treatment of glass fibres on the dynamic mechanical properties of epoxy resin composites. *Compos Part A: Appl Sci Manuf* 1999; 30(8): 997–1002.
51. Verma D, Goh KL and Vimal V. Interfacial studies of natural fiber-reinforced particulate thermoplastic composites and their mechanical properties. *J Nat Fibers* 2020: 1–28.
52. Schadler L and Galiotis C. Fundamentals and applications of micro Raman spectroscopy to strain measurements in fibre reinforced composites. *Int Materials Reviews* 1995; 40(3): 116–134.
53. Filliben JJ. The probability plot correlation coefficient test for normality. *Technometrics* 1975; 17(1): 111–117.
54. Pyke R. Spacings. *J R Stat Soc Ser B (Methodological)* 1965; 27(3): 395–449.
55. Holst L. On the lengths of the pieces of a stick broken at random. *J Appl Probab* 1980; 17(3): 623–634.
56. Kotz S, Johnson N and Read C. *Encyclopedia of Statistical Sciences*, 1988.
57. Feih S, Wonsyld K, Minzari D, et al. *Testing Procedure for the Single Fiber Fragmentation Test*. Roskilde, Denmark: Riso National Laboratory, 2004.

Appendix

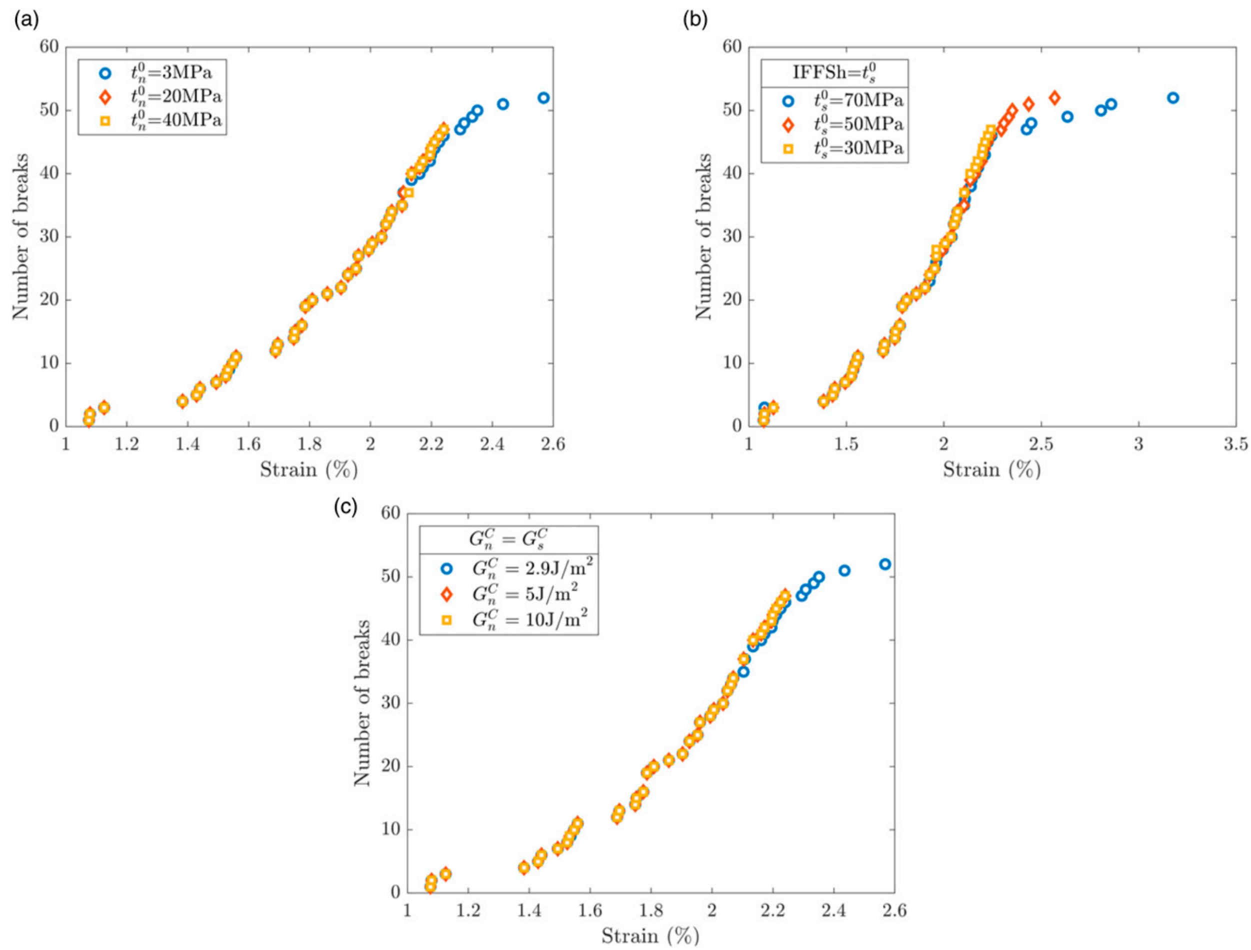

Figure A1. Parametric study indicating the effect of interface failure upon the fibre break evolution during the test (i.e., on number of breaks versus strain): (a) influence of normal strength t_n^0, (b) influence of interfacial shear IFFSh or t_s^0 and (c) influence of critical energy $G_n^C = G_s^C$, (taking the shear and normal critical as equal).